Chapter 2

Site Description, Measurement Techniques and Data Analysis

This chapter provides an overview of the study areas and the datasets from ground-based and satellite remote sensing instruments that are used in this study. The datasets have been taken over three regions (i) the tropical urban station of Hyderabad located in central-south India, (ii) the Bay of Bengal (BoB) during the Winter Integrated Campaign for Aerosols Trace Gases and radiation Budget (W-ICARB) and (iii) the South Asian region covering peninsular India, Arabian Sea (AS), BoB and Northern Indian Ocean (NIO). Continuous ground-based measurements of aerosol mass concentration, particle size distribution, Black Carbon (BC) aerosols, AOD, vertical profile of aerosols and trace gases have been carried out in the premises of National Balloon Facility of Tata Institute of Fundamental Research (NBF-TIFR) campus (17.28^0 N, 78.56^0 E, 545 m amsl) located at ~15 km from the northeast edge of the Hyderabad city, using various instruments such as optical particle counter (OPC), Quartz Crystal Microbalance (QCM), Aethalometer, Microtops-II sun photometer, Multi Wavelength Radiometer (MWR), Micro-Pulse Lidar and trace gas analyzers. Since the aerosol properties over Hyderabad are highly influenced by long range transport from adjoining ocean and Indian peninsula, this thesis also includes the study over BoB during W-ICARB campaign. The measurements of surface, vertical (upto ~1km) and columnar aerosol properties were carried out in the marine atmospheric boundary layer (MABL). Data base from MODIS-Terra sensor is used to understand the spatial distribution of aerosols properties over South Asia. Detailed description of study areas datasets and instruments used in this thesis is given in the following sections.

2.1 Site Description, Regional and Synoptic Meteorology

Hyderabad is the 5^{th} largest city in India extending from 17.17^0 - 17.83^0 N to 78.17^0 - 78.83^0E. The metropolitan area includes twin cities viz. Hyderabad and Secunderabad with its suburbs extending up to 16 km. The rate of urbanization in Hyderabad city has been very rapid since 1960. The population of Hyderabad has increased from 0.448 million in 1901 to 7.75 million in 2011. However, the decadal growth of population has been decreased from (1991-2001) to (2001-2011) which is much lower than the population decadal growth rate of 11.10% for the Andhra Pradesh

state. As the city has grown up rapidly over the years the quality of environment has declined steadily. In recent years unrestrained industrialization in certain sectors and a large increase in traffic have both contributed significantly to the deterioration of air quality, thus making assessment of air quality in selected areas necessary.

The climate of the study area follows the Indian monsoon system with generally a dry season during winter (December to February) and pre-monsoon (March to May) and a wet season in monsoon (June to September). Post-monsoon (October-November) is a transition season with sparse rainfall. More than 75% of the rainfall occurs during the southwest monsoon season (June to September) when the Relative Humidity (RH) is very high. The majority of the aerosol measurements were carried out at NBF-TIFR during the two-year period 2008 and 2009 along with simultaneous measurements of the meteorological variables. The annual variation of the meteorological parameters is shown in Fig. 2.1.1 (a-d). The mean air temperature is high ranging from 21 ^{o}C in December to 33 ^{o}C in May, while during monsoon it decreases (25 - 28 ^{o}C) due to increased rain fall and cloudiness. The RH exhibits high values (up to 70%) in the monsoon season, while in March-May it is the lowest (35-40 %). The atmospheric pressure has lower values during monsoon (not shown) suggesting the uplift of moist air masses and release of precipitation. Precipitation is nearly absent in winter and pre-monsoon, but is significant due to rainfall in February and March of 2008. In contrast during late monsoon (August-September) the rainfall is high reaching a peak of 470 mm in August of 2008 reducing afterwards. A large variability in the rainfall amounts between the two contrasting monsoon years is seen in the Fig. 2.1.1c, that caused significant variations in aerosol load and properties. The flow chart of the wind speed (WS) and direction on seasonal basis is shown in Fig. 2.1.1 (d). The WS is generally low (< 5 m s^{-1}) in all seasons enhanced in late pre-monsoon and monsoon to values up to 7 ms^{-1}. During pre-monsoon and monsoon seasons the higher WS is mainly in northwest and southwest directions respectively carrying significant amount of dust aerosols (from Arabian Peninsula, Middle East and Thar desert) mixed with marine air masses (from AS and Indian Ocean) and local pollution on certain cases (Kaskaoutis et al., 2009). In contrast during post-monsoon and winter seasons the winds flow from northeastern directions mainly and are generally dry and rich in continental aerosols with a large fraction of fine and coarse mode particles from Indo-Gangetic Plains (IGP) and BoB.

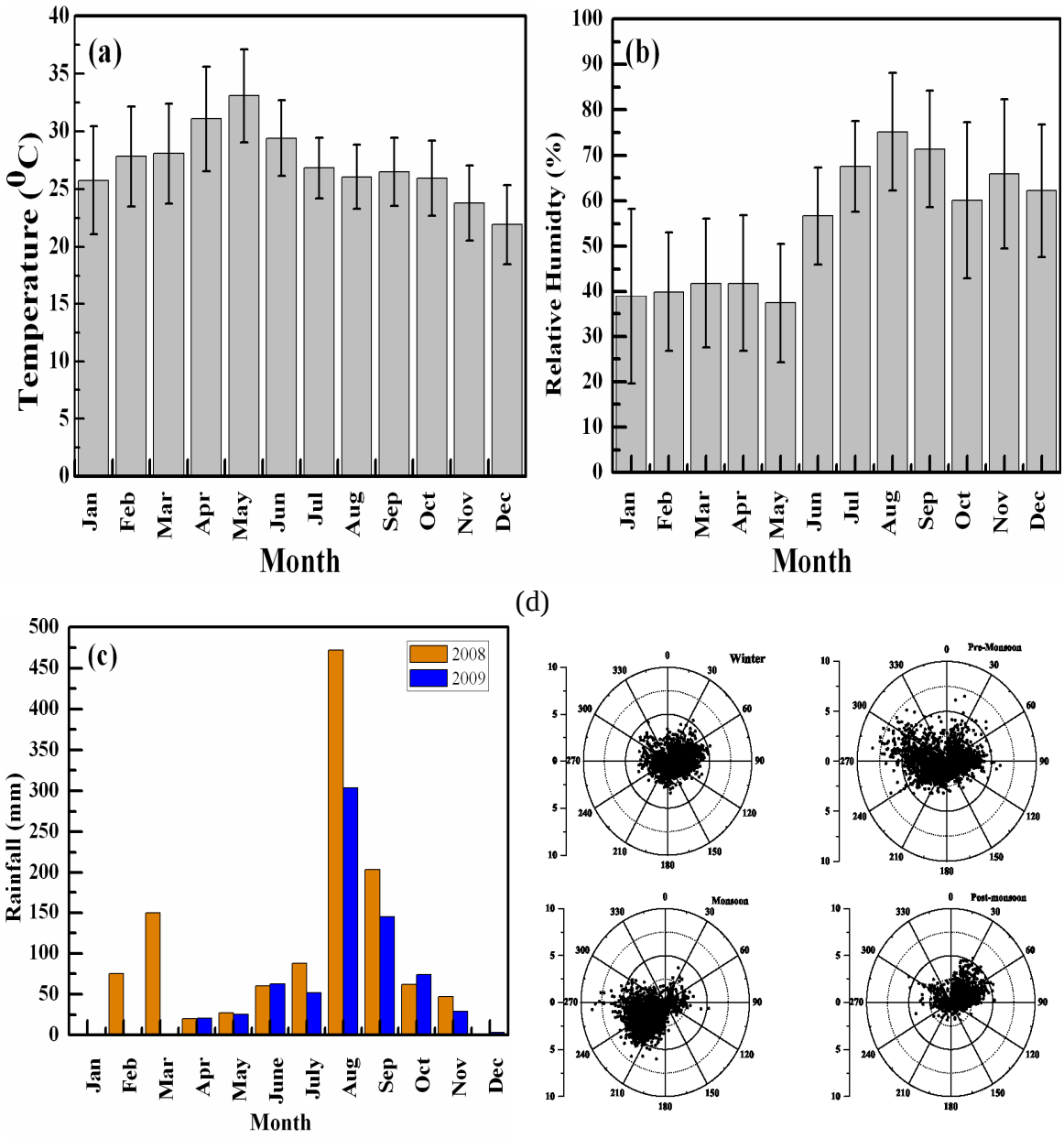

Figure 2.1.1: *Annual variation of air temperature (a), relative humidity (b) and monthly accumulated precipitation over Hyderabad during 2008-2009. The vertical bars express one standard deviation from the monthly mean. (d) Flow chart of the seasonal variation of wind speed and direction over Hyderabad during the period of Jnauary2008 to December 2009. [Winter: December-February, Pre-monsoon: March-May, Monsoon: June-September, Post-monsoon: October-November].*

The surface and columnar aerosol properties over Hyderabad are highly influenced during winter, Pre-monsoon and Monsoon seasons as being in the downwind region of IGP, BoB, AS and NIO. The northern part of India is crossed by the Ganges river; the region is surrounded by the

towering Himalayas in the north, the Thar desert in the west, Vindhayan hill in the south and the BoB in the east. This area is known as IGP accounting ~21% of the land area of the Indian sub-continent and holding nearly 40% of the total population (Badarinath et al., 2011). Several industries and thermal power plants are located in the IGP contributing to significant aerosol and pollution emissions (Reddy and Venkataraman, 2002). During winter season the area is influenced by severe fog and haze conditions causing pollution smog environment. BoB is a closed oceanic area located from ~8^{o}N to ~21^{o}N (Ganges-Brahmaputra delta) and it has a unique weather pattern apart from the regular Indian monsoon, it is also the site for the origin of tropical cyclones (Badarinath et al., 2009). It is surrounded by the rapidly developing South Asian countries including India, Bangladesh, Myanmar Thailand and Indonesia. The BoB being surrounded by densely populated and industrialized regions that affect the aerosol population mix over the entire BoB. The continental aerosols transported over BoB are of various types such as dust particles, fossil-fuel combustion, biomass burning and therefore effects the chemical and optical properties in spatial and temporal domains (e.g. Kumar et al., 2010; Kaskaoutis et al., 2011). The western and northern BoB are strongly affected by the Indian landmass, while the eastern part is mainly under the influence of the Southeast Asia (Moorthy et al., 2010). The Arabian Sea is surrounded by arid and semi-arid regions which are a source of wind-blown dust particles as well as anthropogenically-produced sulfate and carbonaceous particles (Krishnamurthy et al., 1998). The Arabian Sea is under the strong influence of the local monsoon system particularly during monsoon when strong southwestern marine winds in the lower troposphere blows towards Indian mainland, while westerlies bring large amounts of dust in the middle and upper troposphere over Arabian Sea. During transition of monsoonal flow from the northeast to southwest brings dry continental air over the Northern Indian Ocean which leads to a low level temperature inversion, mostly clear skies with scattered cumuli and minimal rain fall. This in turn enables the haze laden with pollutants to accumulate and spread on the ocean basin scale (Ramanathan et al., 2001). Han et al. (2010) reported that sea level has decreased substantially in the south tropical Indian Ocean whereas it has increased elsewhere and attributed that this pattern is driven by changing surface winds associated with a combined invigoration of the Indian Ocean Hadley and Walker cells, patterns of atmospheric overturning circulation in the north–south and east–west direction, respectively, which is partly attributable to rising levels of atmospheric greenhouse gases.

South Asia is the most densely populated area over the globe and also considered as one of the most polluted zone. Due to dramatic increase in population, industrialization and energy demands, atmospheric aerosols and pollutant emissions have gradually been increasing over South Asia (Lawrence and Lelieveld, 2010 and references therein). The outflow of these aerosols and pollutants over the adjoining oceanic regions and Himalayan range has caused dramatic effects in regional climate associated with the formation of atmospheric brown clouds (Ramanathan et al., 2007), precipitation re-distribution (Lau et al., 2006), impact on monsoon onset (Gautam et al., 2009a), mid-tropospheric heating (Gautam et al., 2010) and intensity of the solar dimming phenomenon (Kambezidis et al., 2012). The general meteorology of South Asia region is controlled by the Asian monsoon circulation and it also follows the similar climatology as described earlier for Hyderabad. The seasonal and annual variations of the Asian monsoon circulation have the great impact in the societal development and economic prosperity over the region. One of the important factors that influence the Asian monsoon is the Inter Tropical Convergence Zone (ITCZ) which is the convergence of the trade winds of the two hemispheres. The seasonal migration ITCZ has an important role in the transportation and distribution of aerosols and trace gases over the South Asia (Lawrence and Lelieveld, 2010).

2.2 Instruments and Data Analysis

For the present study, both the ground-based and satellite data have been used. A detailed description of each instrument as well as the methodology of the data analysis and the retrievals is given in the following:

2.2.1 Multi-Wavelength Radiometer

Multi-Wavelength Radiometer (MWR) was used for aerosol retrievals over Hyderabad which provides real-time measurements of the relative flux of direct-beam solar radiation at the Earth's surface as a function of solar zenith angle for 10 selected wavelengths centered at 380, 400, 450, 500, 600, 650, 750, 850, 935 and 1025 nm. The wavelengths are selected using narrow band interference filters having 5-nm full width at half maximum bandwidth, a peak transmittance >30% and a band shape factor of 3 ensuring a near uniform transmittance within the pass-band and a sharp reduction in the transmission beyond. The radiation is passed through a field-limiting optics that limits the total field of view of the instrument to $<2^{o}$. The radiant energy at different

wavelength is isolated by filters arranged in a rotating filter wheel. The sequencing of filters and solar tracking is accomplished by DC driven motor and equatorial mounting i.e. having one rotational axis parallel to the Earth's axis of rotation. In addition to the interference filter a neutral density (ND) filter is also attached in the optical path of the system for the calibration gain selection and testing. An incident solar flux passing through the filters is converted into the electrical signal by means of photo-detector. Measurements were carried out under cloudless sky conditions. The measured spectral solar radiation are then used to derive the spectral AOD, columnar aerosol size distribution (CSD) and several other parameters related with particle size i.e. Ångström exponent, effective radius etc. The transmitted direct-beam solar irradiance from the atmosphere incident on the photo-detector is given by the Bouguer-Lambert-Beer law:

$$F_\lambda = (\frac{R_m}{R})^2 F_{0\lambda} e^{-m(\theta)\tau_\lambda} \tag{2.2.1}$$

Where $F_{0\lambda}$ is the solar irradiance at zero air mass (top of atmosphere) at wavelength λ, R_m and R are the mean and the actual Sun-Earth distance respectively, $m(\theta)$ is the relative air mass at solar zenith angle θ and τ_λ is the total optical depth at λ. The radiometer output voltage V(λ, θ) is linearly related to observed ground level solar flux F_λ and therefore the total optical depth can then be determined by taking the slope of a straight line fitted to the data points having ordinate values of lnV(λ, θ) and abscissa values of $m(\theta)$:

$$\ln V(\lambda,\theta) = 2\ln(\frac{R_m}{R}) + \ln V_0(\lambda) - m(\theta)\tau_\lambda \tag{2.2.2}$$

In order to account the Earth's curvature effect and atmospheric refraction the empirical relation for the relative air mass is given by Youg (1994) as:

$$m(\theta) = \frac{0.0096467 + 0.148386\cos\theta + 1.002432\cos^2\theta}{0.000303978 + 0.0102963\cos\theta + 0.149864\cos^2\theta + \cos^3\theta} \tag{2.2.3}$$

For solar zenith angles smaller than ~70^0 equation (2.2.3) can be approximated by m = secθ.

The total optical depth $\tau(\lambda)$ includes the contribution from air-molecules, aerosol extinction, ozone, water-vapor and trace gases absorption and can be expressed as:

$$\tau_\lambda = \tau_R(\lambda)\frac{P}{P_0} + \tau_a(\lambda) + \tau_g(\lambda) + \tau_{O3}(\lambda) + \tau_w(\lambda) \tag{2.2.4}$$

Where $\tau_R(\lambda)$ is the molecular scattering optical depth for a standard atmosphere (Rayleigh scattering), P and P_0 the atmospheric pressure at the measurement site and at mean sea level

(1013.25 hPa) respectively, $\tau_a(\lambda)$ is the optical depth due to aerosol extinction (scattering and absorption), $\tau_g(\lambda)$ is the optical depth due to mixed and trace gases absorption i.e. O_2, N_2, NO_x, etc, $\tau_{O3}(\lambda)$ is the optical depth due to ozone absorption (UV and Chappuis band) and $\tau_w(\lambda)$ is the optical depth due to water-vapor absorption bands in the NIR. From equation (2.2.4) the aerosol extinction can be obtained as:

$$\tau_a(\lambda) = \tau(\lambda) - \tau_R(\lambda)\frac{P}{P_0} - \tau_g(\lambda) - \tau_{O3}(\lambda) - \tau_w(\lambda) \quad (2.2.5)$$

The derivation of spectral AOD is done using Langley plot technique which initially can be considered as a first validation of the accuracy in $\tau(\lambda)$. This technique is based on equation (2.2.2) using a graphical method in which $\ln V(\lambda,\theta)$ is plotted against $m(\theta)$. The $\ln V_0(\lambda)$ and $\tau(\lambda)$ represent the intercept and slope of the straight line respectively. The accuracy of the $\tau(\lambda)$ depends on the linear regression fit and the stability of the intercept value. A typical example of the application of Langley technique at each of the 10 MWR wavelengths is shown in Fig. 2.2.1 for the 1st May 2008 where the retrieval of $\tau(\lambda)$ is very accurate for all wavelengths. Furthermore, the accuracy in spectral AOD retrievals depends on the quantitative estimation of the contribution of the other parameters in equation (2.2.5). The typical error in the retrieved AOD is ~0.01, excluding the variance of the Langley fit. The variance of the Langley intercept (typically 5%) along with other uncertainties influence of Rayleigh scattering and absorption by ozone and trace gases increases the uncertainty in AOD in the range of 0.02-0.03. The optical depth due to ozone absorption was estimated in the band 450-700 nm using spectral absorption cross section from MODTRAN and the tropical altitude profile of ozone. The uncertainties in the AOD for subtracting the ozone absorption are very small (<0.003). Other smaller uncertainties are due to trace gases, mainly NO_2 which is determined through the NO_2 concentration. The Rayleigh scattering component proposed as by Gueymard (1995) is given bellow

$$\tau_{R\lambda} = 0.008735(P/P_0)\lambda^{-4.08} \quad (2.2.6)$$

The 935-nm channel was used for estimating the columnar water vapor (CWV), along with the window channel of 1025 nm; these records were also used to correct for water vapor absorption at 850 nm which is ~0.005 (Gogoi et al., 2009). The presence of clouds mainly in monsoon limits the radiation measurements. This study mainly focused on the monthly averages and seasonal patterns of aerosol properties and thus a sufficient number of spectral AODs are available for each month except for the month of July that was omitted from the analysis. In this study a total of 410 sets of

MWR data spread over 2 years (January 2008-December 2009) have been analyzed to obtain the aerosol characteristics and radiative forcing over Hyderabad on monthly and seasonal basis that are discussed in Chapter 3 and 6 respectively.

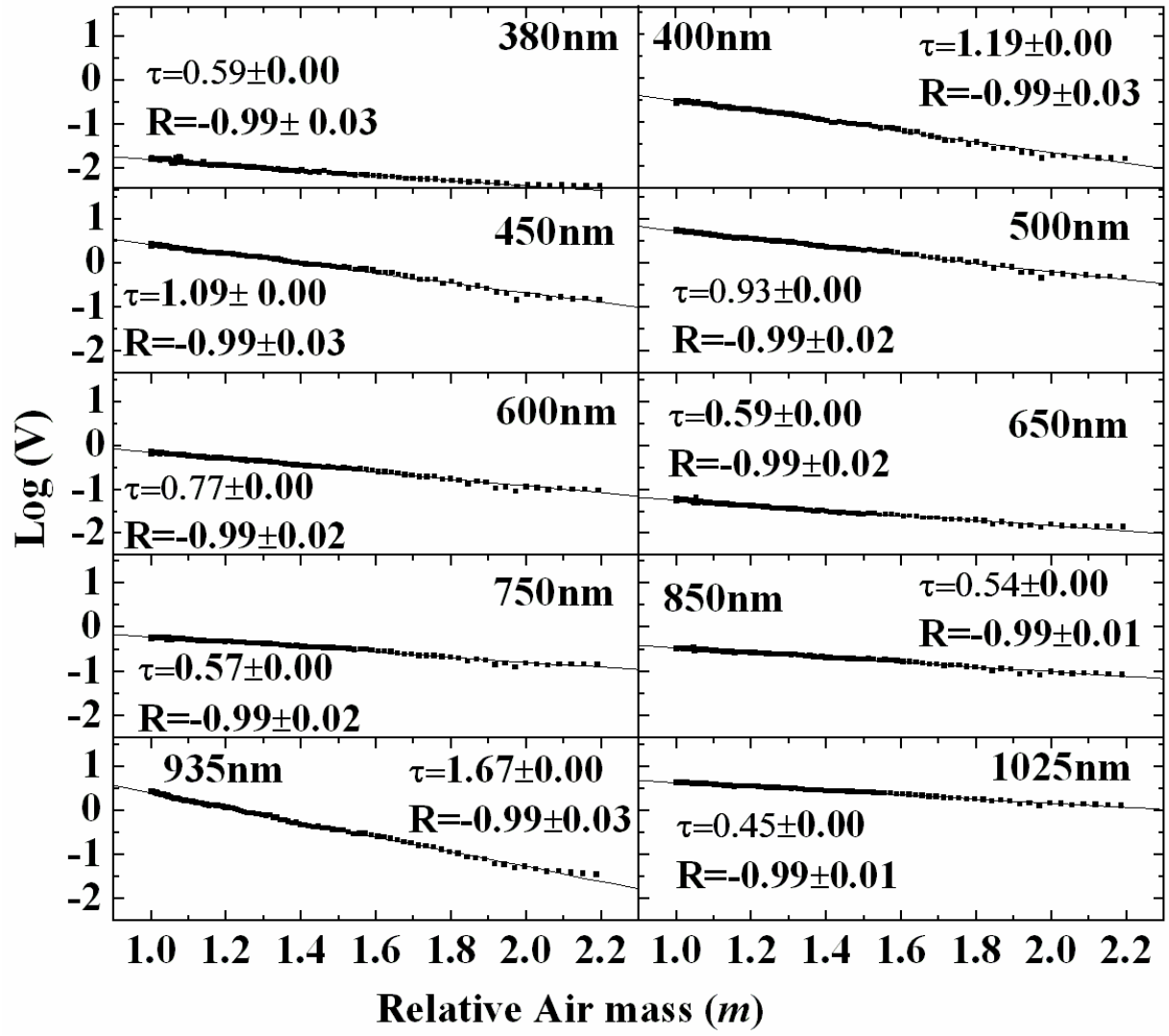

Figure 2.2.1: *Langley plot from MWR data on 1st May 2008 over Hyderabad. The points are the individual measurements and the straight line is the linear least square fit to the data. The values of total optical depth and the correlation coefficient are shown in each panel along with the wavelength.*

The spectral dependence of AOD contains valuable information about the physical and optical properties of aerosols and can be simulated by the Ångström power law (Ångström, 1964):

$$\tau_{\alpha\lambda} = \beta\lambda^{-\alpha} \quad (2.2.7)$$

Where α is the wavelength exponent which is an indicator for the particle size and fine-mode fraction to the total AOD (Schuster et al., 2006) while β (equals to AOD at λ=1 μm) is the turbidity

coefficient providing a measure of columnar aerosol loading. The values of α and β have been estimated using the least square fit using the lnAOD vs lnλ plot in the wavelength range 400-1025 nm:

$$\ln AOD_\lambda = -\alpha \ln\lambda + \ln\beta \quad (2.2.8)$$

A similar procedure was followed for the calculation of α and β using Microtops-II sun photometer which will be discussed in next section. In the equation (2.2.7) α and β are considered independent to each other and to the wavelength used for their determination however, it has shown that both α and β depend strongly on the wavelength band of the measurements (Kaskaoutis and Kambezidis, 2008). Also the validity of the Ångström's formula is based on the Junge (1955) power law; for the monomodal aerosol size distribution in the atmosphere. However, it is well known that aerosol size distribution in the atmosphere is in general bi-modal in nature and deviates significantly from the Junge expression (Eck et al., 1999). As a consequence, the Ångström's formula (equation 2.2.7) exhibits some deviations in $\ln(AOD_\lambda)$ vs. $\ln(\lambda)$ plot which reveals a curvature in equation (2.2.8); thus a more precise relationship between AOD_λ and wavelength is obtained using a second-order polynomial fit expressed as:

$$\ln AOD_\lambda = \alpha_2(\ln\lambda)^2 + \alpha_1 \ln\lambda + \alpha_o \quad (2.2.9)$$

Where the coefficient α_2 accounts for a curvature. The curvature can be used as an indicator for the aerosol-particle size, with negative values indicating size distributions dominated by fine-mode aerosols and vice versa (Eck et al., 1999; Schuster et al., 2006; Kaskaoutis et al., 2007).

As the spectral AODs contain an imprint of the CSD, the seasonal mean CSDs were retrieved following the King's numerical inversion using the Mie integral equation:

$$\tau_\lambda = \int_{r_a}^{r_b} \pi r^2 Q_{ext}(m, r, \lambda) n_c(r) dr \quad (2.2.10)$$

Where Q_{ext} is the Mie extinction efficiency which depends on the complex refractive index (m), particle radius (r) and wavelength (λ); $n_c(r)$ is the aerosol columnar number density (in a vertical column per unit cross-section) in the radius range dr centered at r, while the r_a and r_b are the lower and upper cutoff radii of the particles respectively such that the particles within this range contribute almost totally to the observed AOD spectra. Thus r_a and r_b depend on the short and long wavelength limits of the AOD spectra (King 1982). The CSD $[n_c(r)]$ is defined such that the

number size distribution is height invariant or averaged over the vertical column (King et al., 1978). It was retrieved from the spectral AODs by numerical inversion of equation 2.2.10 using the linear inversion method of King et al. (1978). The wavelength dependent complex refractive index given by Lubin et al. (2002), and $r_a =$ 0.05 μm and $r_b =$ 3 μm were used in this study. The spectral AODs are then re-estimated using the direct Mie equation and are compared with the measured ones. The estimated CSDs are accepted only when the re-estimated AODs agree with the measured ones within the measurement errors. As the measurement errors are part of inputs the final solution are weighted by these errors with better accuracy around size ranges sensitive to more accurate AOD measurements (King, 1982). In equation 2.2.10 spherical aerosols are assumed; thus the presence of non-spherical dust particles would deviate the results leading to underestimation of the mean and effective radius.

For describing the radiative transfer properties of aerosols, the area-weighted mean or effective radius (R_{eff}) constitutes a key parameter. R_{eff} is the radius of an equivalent monodispersion system exhibiting the same total scattering with a polydispersive one and is defined as the ratio of the third moment to the second moment of the aerosol number size distribution:

$$R_{eff} = \int_{0.05}^{3} \frac{r^3 n_c(r)\,dr}{r^2 n_c(r)\,dr} \tag{2.2.11}$$

From the retrieved CSDs the columnar number density (N_T) and the columnar mass loading (m_L) of aerosols were also calculated as:

$$N_T = \int_{0.05}^{3} n_c(r)\,dr \tag{2.2.12}$$

$$m_L = \frac{4\pi d}{3} \int_{0.05}^{3} r^3 n_c(r)\,dr \tag{2.2.13}$$

Where d is the mean aerosol density value of 2.2 g cm^{-3} (Pruppacher and Klett, 1978). Furthermore, the columnar amount of accumulation (N_a) and coarse (N_c) aerosols were calculated using as threshold radius the 0.5 μm:

$$N_a = \int_{0.05}^{0.5} n_c(r)\,dr \tag{2.2.14}$$

$$N_c = \int_{0.5}^{3} n_c(r)\,dr \tag{2.2.15}$$

2.2.2 Microtops-II sun photometer

Microtops-II sun photometer (hereafter referred to as MTS) is the manual operating instrument that measures the direct-beam irradiance at 7 wavelengths; six of them (380, 440, 500, 675, 870, 936 and 1020nm) are used for aerosol retrievals, while the 7^{th} at 936 nm for retrieval of water vapor content (WVC). MTS measures the direct-beam irradiance under cloudless skies and calculates the spectral AODs from the respective radiation intensities at top-of-atmosphere using its internal calibration for each channel. The Langley technique as discussed in previous section is also applicable for MTS to derive the spectral AOD. The number concentrations of H_2O, O_3, O_2 and N_2 and air column density of $2.16x10^{26}$ moles cm^{-2} for tropical atmosphere have been used in order to account for Rayleigh scattering and gaseous absorption. The Full Width at Half Maximum (FWHM) bandwidth for 380nm channel is 2.4±0.4 nm and 10±1.5 for other channels. The accuracy of the sun-targeting angle is better than 0.1^o, while the field of view (FOV) is 2.5°.

Typical errors in AOD measurements from MTS are ~0.03 (Morys et al., 2001) with larger values in the UV, while errors from the subtraction of Rayleigh component, ozone and water-vapor absorption are lower of the order of one magnitude. Shaw (1980) reported anomalous absorption at 1010 nm due to water vapor, since the extinction at this wavelength increases with increasing columnar water vapour (CWV). The water-vapor absorption also affects the measurements at 1020nm and increases the measured AOD from MTS. There is another possible uncertainty associated with the 1020nm channel due to the temperature sensitivity of the silicon detector which is insignificant for the other channels (Kaskaoutis et al., 2010). MTS data was collected every 30 minutes during the period of April 2009 to March 2010.

2.2.3 Aethalometer

Continuous real-time measurements of the Black Carbon (BC) aerosol mass concentration and absorption coefficient were carried out since January 2009 at NBF-TIFR using seven wavelengths Aethalometer (model AE-42). A semi-continuous optical absorption method is applied to measure the attenuation of light by aerosols at the seven selected wavelengths (370, 470, 520, 590, 660, 880 and 950 nm) passing through a filter tape first without and then with the aerosol loading. The instrument aspirates ambient air at a standard flow rate of 5 liter per minute from an altitude of ~10 m above the ground level. The measurement sampling interval was kept at 5 minutes. The particles

in the incoming air flow are deposited on the quartz filter tape of the Aethalometer and the BC mass concentration is determined by measuring the change in transmittance through the quartz filter tape due to the particle deposition. The absorption coefficient of aerosols and the BC mass concentration (in μg m^{-3}) are obtained by using Lambert-Beer's equations:

$$\beta_{abs} = \frac{1}{CR} A \ln(\frac{I_0}{I}) / (Q\Delta t) \tag{2.2.16}$$

$$M_{BC}(\lambda) = \frac{\beta_{abs}(\lambda)}{\sigma_{abs}(\lambda)} = \frac{\beta_{abs}(\lambda).C}{\sigma_{atn}(\lambda)} \tag{2.2.17}$$

Where I_0 and I are the light intensities transmitted through the filter matrix before and after particle deposition on it, Q is the volumetric flow rate of air sampled at sampling interval Δt and A is the area of the aerosols deposited on filter spot. C and R are correction factors; C accounts for the effect of multiple light scattering before the deposition of the particles within the filter and shadowing effect (R) the loading of particles in the filter during the measurement. The value of attenuation cross-sections $\sigma_{atn}(\lambda)$ = 14625/λ nm m^2 g^{-1} is used for the BC measurements. For accurate measurements of absorption coefficient and consequently BC mass concentration, the values of the correction factors (C and R) need to be known with higher accuracy. The overestimation of BC mass concentration due to multiple scattering within the filter is partly compensated by higher particle loading in the filter which decreases the optical path. Based on several experiments Weingartner et al., (2003) found that the shadowing effect and R factor are quite significant for pure soot particles, while almost negligible for aged aerosols (mixture of several components). For the mixed aerosols they estimated the C factor to be ~ 2.1. In the present study, the values of R = 1 and C = 2.355, 2.656, 2.677, 2.733, 2.827, 2.933, 2.925 are used for the seven selected wavelengths in Aethalometer measurement following the work by Schmid et al. (2006). The maximum uncertainly in the measured BC was up to 20% (ranging from ~40 ng m^{-3} to 60 ng m^{-3}) with higher percentage of error for low concentrations (Corrigan et al., 2006; Moorthy et al., 2007).

2.2.4 Quartz Crystal Microbalance

An automated Quartz Crystal Microbalance (QCM) cascade impact or (model PC-2HX) was used for size segregated total aerosol mass concentration measurements. The instrument deploys 10 stages with 50% cutoff radii at 10, 5.6, 3.0, 2.0, 1.0, 0.5, 0.3, 0.2, 0.1 and 0.05 μm. It samples

the ambient air through the Teflon tube inlet at a constant flow rate of 2 liter per minute (lpm) and it operates for every 30 minutes during the day time. Before the actual measurement filtered air is flushed in order to attain the crystal stability. Each crystal has its natural resonance frequency of vibration and the mass sensitivity of a vibrating crystal is a function of the square of the resonance frequency as follows:

$$\Delta F = 2.2x10^{-6} f^2[\frac{\Delta m}{a}]$$
$$\Delta m = 1.44.\Delta F$$
$$C_i = K_i[\frac{\Delta F}{\Delta t}] \quad (2.2.18)$$

Where ΔF is the frequency change due to particle deposition, Δm is variation in the mass, a the electrode area of 0.377 cm^2, f the crystal resonate frequency of 10^7 Hz, C_i the mass concentration, K_i the sensitivity constant and Δt the sampling interval. If ΔF =1, Δm =1.44ng implying that 1.44 ng of particles is deposited on crystal inducing a change of 1Hz in it.

During each measurement relative changes in frequency between the sampling and reference crystals are recorded as a function of time and the composite aerosol mass concentration is calculated using equation 2.2.18 by assuming a particle density of 2 gcm^{-3}. The size-segregated aerosol mass concentrations are used in combination with BC mass measurements for estimating the BC mass fraction (*described in section 4.1.2*). The measurements are restricted for atmospheric conditions with RH< 75 % in order to avoid aerosol growth from the humidification. The RH is continuously recording at the station and the QCM measurements are stopped in cases when RH exceeds 75-78 %. The uncertainties in the aerosol mass concentrations are in the range of 10% to 20% at very low mass concentrations (~10 μg m^{-3}) and the error reduces to <10% for high mass concentrations >30 μg m^{-3} (Nair et al., 2009).

2.2.5. Optical Particle Counter

Optical particle counters (OPC) can provide rapid real-time monitoring of the particle number concentration by optical sizing the particles in a volume controlled flow. Size-segregated aerosol number concentrations were measured in 15 size bins in the diameter range 0.3-20 μm using optical particle counter (GRIMM 1.108) at 5 minute sampling time interval. The OPC was used for the measurements of aerosol size distribution for all the 35 days during the W-ICARB cruise

campaign. The sampling instrument aspirates the ambient air through an isokinetic community air inlet pipe fixed to the port side of the ship at the rate of 1.2 lpm and it performs self-test and zero calibration check at the beginning of each measurement. The instrument uses a light-scattering technique for single-particle counts, whereby a semiconductor laser serves as the light source, while is capable of counting from 1 particle L^{-1} to 2 million particles L^{-1}. Each particle is sized based on the amount of incident light scattered and the proper mass concentration is established by calibrating the instrument with the Latex (polystyrene latex) for particle sizing having a complex refractive index of 1.60 + 0i. The disadvantage of this instrument is that the measurements are limited in the size range 0.3 to 20 µm and therefore, all analyses are truncated in this range missing out particles below 0.3 µm. This fact affects the measured aerosol number size distribution and the simulated distributions in the fine and nucleation modes.

The accurate measurement and control monitoring of aerosol using OPC depends on the ambient temperature, relative humidity (RH) and pump flow rate. The temperature and RH range for the smooth operation of the instrument is 0-40^{0}C and <95% respectively. A major task that must be taken into account in aerosol measurements is the hygroscopic growth of the particles. Rissler et al. (2006) have investigated the hygroscopic growth of aerosols in the Amazon and found no step-like deliquescent behavior of the aerosol in the dry and wet period. The particle growth factor (g_f) can be described as:

$$g_f = [1 + p(\frac{RH}{100}) / 1 - (\frac{RH}{100})]^{\frac{1}{3}} \quad (2.2.19)$$

Where p takes a value of ~0.1 for the most hygroscopic particles. It was reported that the hygroscopic growth of the most water-soluble particles is 1-2% for the RH range of 70-80%, while the error in aerosol number concentration measurements will be <10% due to hygroscopic growth (Fairall, 1984; Kowalski, 2001; Vong et al., 2004). OPC was also deployed in W-ICARB cruise campaign over BoB. During the W-ICARB cruise the RH exceeded 70-80% on only few days when the ship was crossing the southernmost BoB and NIO. Therefore, the errors in the OPC measurements due to hygroscopic growth factor is limited over a small area and is not considered significant, since the RH did not exceed 80%.

2.2.6 Micro-Pulse Lidar

A portable Micro-Pulse Lidar (MPL) system has been operating from April 2009 at NBF- TIFR during late-evening hours (after sun set) under cloudless conditions on specific days (every Wednesday following international protocol of Geophysical day). The Lidar has the potential capability to detect the structured layers of aerosols from near surface to middle and upper troposphere and can also identify several dynamical parameters of the atmospheric boundary layer (ABL) such as boundary layer height (BLH) and depth of entrainment zone. Lidar employs high pulse repetition rate and low power transmission technique.

The operating characteristics of the MPL are summarized in Table 2.2.1. This MPL is operating at 532 at transmitted energy of 10 μJ with a pulse repetition frequency of 2.5 kHz. The laser system bin width was set at 200 ns corresponding to a vertical resolution of 30 m. The laser beam diameter is 0.4 mm and its divergence less that 1.5 mrad. The laser beam was expanded to 3 mm and collimated to have the beam divergence of ~200 mrad. The light output is linear with polarization degree greater than 99%.

Table 2.2.1 *Operating characteristics of the Micro Pulse Lidar (MPL).*

Transmitter		***Receiver***	
Pulse Energy	10μJ	**Type**	Cassegrain
Pulse Repetition rate	2.5kHz	**Diameter**	15 cm
Pulse Duration	<10ns	**Telescope F-ratio**	9
Beam Divergence	<1.5mrad	**Filter Bandwidth**	0.5 nm
Wavelength	532 nm	**Field of view**	<400 mrad
Polarization	Linear	**Quantum Efficiency**	<10%
Range resolution (height interval)	30m		

The power of the analog signal detected by the lidar detector after elastic scattering due to presence of the air molecules and aerosols can be expressed as:

$$P(r) = P_L a \frac{\eta(r)}{R^2} \beta(r) C(r) \frac{cl}{2} e^{[-2\int_0^h \alpha(r)dr]} \tag{2.2.20}$$

where P_L is the emitted laser power, a the area of receiver of the telescope, $\eta(r)$ the spectral transmission factor, $C(r)$ is the overlap factor between the field of view of the telescope and the laser beam, c the speed of light, l the laser pulse length, R the range and α(r) and β(r) are the range dependent volume back scatter coefficient which can be further expressed as:

$$\alpha(r) = \alpha_{aer}(r) + \alpha_{mol}(r) \tag{2.2.21}$$

$$\beta(r) = \beta_{aer}(r) + \beta_{mol}(r) \tag{2.2.22}$$

Where the subscription "aer" and "mol" are for aerosol and molecules respectively. The vertical profile of the backscattered signal is calculated using the inversion method of Klett (1981) and Fernald (1984) as:

$$\beta_{aer}(h) + \beta_{mol}(h) = \frac{S(r)\exp\{-2\int_{R_0}^{R}[L_{aer}(r) - L_{mol}(r)]\beta_{mol}(r)dr\}}{\frac{S(R_0)}{\beta aer(R_0) + \beta_{mol}(R_0)} - 2\int_{R0}^{R} L_{aer}(r)S(r)T(r,R_0)dr} \tag{2.2.23}$$

The Lidar Ratio (LR) is defined as the ratio of the backscatter to the extinction coefficient as:

$$L_{aer}(r) = \frac{\alpha_{aer}(R)}{\beta_{aer}(R)} \tag{2.2.24}$$

and

$$T(r,R_0) = \exp\{-2\int_{R_0}^{R}[L_{aer}(r') - L_{mol}(r')]\beta_{mol}(r')dr' \tag{2.2.25}$$

The upper limit of R_0 is chosen at 8 km where the aerosol contribution is negligible compared to air molecules (Leon et al., 2009). The molecular lidar ratio $L_{mol}(r)$ is $8\pi/3$ sr^{-1}.

Geometrical Correction

Although MPL uses a co-axial geometry and the laser beam of the transmitter overlaps almost perfectly with the receiver's field-of-view (FOV), an optical range still exists within which the back scattered radiation is not completely overlapped by the receiver's FOV. The imperfect overlap causes some uncertainties that have to be corrected particularly for the detection of lower level aerosols. With the assumption of horizontal homogeneity of the atmosphere (few meters from the ground) the range-corrected backscatter signal should to be uniform if the overlap is perfect, while any deviation from this corresponds to incomplete overlap. For determining the overlap

correction, the MPL was kept horizontally at 30 m above the ground and the horizontal atmosphere was assumed to be homogeneous. The minimum distance for full overlap is found to be 105m which is the minimum operating height of the MPL.

Estimation of lidar ratio and extinction coefficient

Since MPL initially measures the backscatter coefficient the lidar equation (2.2.22) has to be solved to calculate the aerosol extinction coefficient with the arbitrary selection of LR. With this arbitrary selection of LR value, the AOD is calculated from vertical integrated extinction coefficient that matches the AOD derived from MTS during daytime and get the best fit value of LR. The lidar-derived extinction is then weighted by AOD at 532 nm in order to minimize the error associated with the LR assumption, since Kovalev (2004) showed that inappropriate LR values may alter the retrievals under inhomogeneous atmospheres. The LR is strongly dependent on the size, refraction index, shape and composition of aerosols (He et al., 2006) and provides valuable information about the aerosol types (Barnaba et al., 2007; Müller et al., 2007).

2.2.7 Radiosonde

Radiosondes measurements are used to monitor the boundary-layer dynamics and to understand the distribution of vertical profiles aerosol in the atmosphere. Several meteorological parameters such as temperature, pressure, relative humidity (RH), wind speed (WS) and direction (WD) are being measured in every 15 day during 2009-2010 at NBF- TIFR using RS80-15N GPS radiosonde. The uncertainty in temperature measurements is ±0.3 ^{0}C, while it is ±0.5 hPa for atmospheric pressure below 20km. The accuracy of RH measurements depends upon ambient temperature as well as altitude and it varies from ±2 % near the surface to ±15-20 % between 5 and 15 km. The surface meteorological parameters are measured in BF- TIFR using Automatic Weather Station (AWS).

2.2.8 Moderate Resolution Imaging Spectroradiometer

Moderate Resolution Imaging Spectroradiometer (MODIS) is a key instrument aboard the Terra and Aqua satellites. Terra was launched by NASA in December 1999 and Aqua in July 2002. Terra has a southward orbit crossing the equator at 10:30 LST, while Aqua passes the equator northwards at 13:30 LST (Levy et al., 2007). MODIS sensor provides data on high radiometric sensitivity in 36 spectral bands ranging from 0.4 µm to 14.4 µm with 29 spectral bands at 1km, 5

spectral bands at 500m and 2 spectral bands at 250m spatial resolution. A nearly global image is produced daily due to the wide swaths of 2330 km. Aerosol retrievals from MODIS data are performed over land and ocean surfaces using two different algorithms described in literature (Kaufman and Tanré, 1998). The aerosol properties are derived by the inversion of the MODIS observed reflectance using pre-computed radiative transfer look-up tables based on aerosol models (Remer et al., 2005; Levy et al., 2007). The uncertainty associated in the MODIS retrieved with AErosol RObotic NETwork (AERONET) and found to be $\Delta\tau = \pm (0.05+0.15\tau)$ over land and $\Delta\tau = \pm (0.03+0.05\tau)$ over ocean (Remer et al., 2008).

2.2.9 Multi-angle Imaging Spectroradiometer

The Multi-angle Imaging Spectroradiometer (MISR) flies on the Terra platform at an altitude of 705 km above sea level on a sun-synchronous orbit and continuously monitoring AODs globally at nine distinct zenith angles ranging from 70^0 backward to 70^0 forward in four spectral bands centered at 446, 558, 672 and 866 nm and nine cameras at view angles of ±26, ±45 and ±70. It takes 9-days to cover entire globe because of the narrow swath width of 360 km. A lookup table approach is used for aerosol retrieval. In this approach the observed radiance (energy per unit area, wavelength and solid angle) are compared with the simulated top of the atmosphere equivalent reflectances from different aerosol components and models and best fitting models are presented as successful retrievals. The uncertainty associated with MISR derived AODs was found to be about 0.05 and 0.08 for 52.8 km and 17.6 km spatial resolution respectively (Martonchik et al., 2004).

2.3 Atmospheric Models

Due to the large variety in aerosol properties, types, sources and sinks as well as the mixing (internal and external) and transport processes in the atmosphere it is difficult to identify a specific aerosol type from ground based and remote sensing instruments. it is impossible to monitor the aerosols on the global scale due to spatial limitation of the ground-based aerosol network,. For this reason several chemical transport models have been developed in recent years, which simulate the aerosol properties, types and also provide the spatio-temporal distribution based on initial aerosol emissions, meteorology and mixing processes in the atmosphere. A brief summary on four aerosol models used in this study is presented below.

2.3.1 Optical Properties of Aerosols and Clouds

Aerosol in the atmosphere is assumed to be a mixture of different components. These mixtures (or components) of aerosol can be provided by the user from the measurements or by the use of typical mixtures which are included in Optical Properties of Aerosols and Clouds (OPAC) model (Hess et al., 1998). OPAC handles a wide range of aerosol components such as soot (BC), water soluble (NH_4^+, Na^+, K^+, Mg^{2+}, Ca^{2+}, Cl^-, NO_3^-, SO_4^{2-} and HCO_3^- etc.; comprises mostly fine mode particles), insoluble (Na, Mg, F, Cl etc.; comprises mostly coarse mode particles), mineral dust (in nucleation, accumulation and coarse modes), sea salt (in accumulation and coarse mode), etc. as well as standard aerosol types such as urban, continental clean, continental polluted, marine clean, marine polluted, desert etc. [Hess et al. (1998)]. The OPAC model provides the optical properties of aerosol (for the measured or model defined mixtures of aerosols) at the solar and terrestrial spectral wavelength range (0.25 to 40μm). The number density of each component is adjusted matching the measured parameters (i.e. spectral AOD, single scattering albedo, asymmetry parameter) with the calculated ones (e.g. Satheesh et al.,2010). Since the hygroscopic growth of aerosols can modify their optical and physical properties, the OPAC data base is provided at eight values of RH (0%, 50%, 70%, 80%, 90%, 95%, 98% and 99%). In this study, the OPAC model is used to simulate the spectral aerosol properties that are used as inputs for the calculation of aerosol radiative forcing.

2.3.2 Santa Barbara Discrete ordinate Atmospheric Radiative Transfer

Santa Barbara DISORT Atmospheric Radiative Transfer (SBDART) is a radiative transfer FORTRAN code that computes plane-parallel radiation transfer for clear and cloudy skies at the surface and within the atmosphere. The radiative transfer equations are numerically integrated with DIScreet Ordinate Radiative Transfer (DISORT), Stamnes et al., (1988). The discrete ordinate method provides a numerically stable algorithm to solve the equations of plane-parallel radiative transfer in a vertically inhomogeneous and non-isothermal atmosphere. The intensity of both scattered and thermally emitted radiation can be computed at different heights and directions. SBDART is configured to allow up to 65 atmospheric layers and 40 radiation streams (40 zenith angles and 40 azimuthal modes). The code is based on a collection of highly developed and reliable physical models which have been developed by the atmospheric science community over the past few decades. More specifically, SBDART has adopted six standard atmospheric profiles

that suite for tropics, mid-latitude summer, mid-latitude winter, sub-arctic summer, sub-arctic winter and US62. These standard model atmospheres provide the vertical profile of pressure, temperature, water vapor and Ozone density. The model also allows including these parameters from radiosonde and Ozonesode observations at the site (Ricchiazzi et al., 1998). The input parameters in the model are the AOD, Ångström exponent (α), single scattering albedo (SSA), CWV and ozone amount. Furthermore, surface reflectance (albedo) is an important parameter for estimation of the aerosol radiative forcing (McComiskey et al., 2008). SBDART suit with the five basic surface types namely ocean water (Tanre et al., 1990), lake water (Kondratyev, 1969) vegetation (Reeves et al., 1975), snow (Wiscombe and Warren, 1980) and sand (Staetter and Schroder, 1978) to parameterize the spectral surface albedo. SBDART also allows the modification of the surface reflection properties by varying the surface conditions as combinations of water, snow, vegetation and sand.

SBDART relies on LOWTRAN7 code which provides the clear-sky atmospheric transmission from 0 to 50 000 cm^{-1} and includes the effects of all atmospheric radiatively active molecular species (Ricchiazzi et al., 1998). The aerosol models adopted in SBDART are taken from those provided in the 6S (Tanre, 1988) and LOWTRAN7 codes (Shettle and Fenn, 1975). The SBDART was used for the computation of aerosol radiative forcing and atmospheric heating rates over Hyderabad (*described in section 6.2*).

Aerosol Radiative Forcing

The term aerosol radiative forcing (ARF) includes the perturbation in the Earth's radiation budget caused by atmospheric aerosols by scattering and absorption of incident solar radiation. The ARF is considered both for the shortwave (solar) radiation (0.3 - 4.0 μm) and for the longwave radiation (4 - 100 μm). The ARF is considered at surface, within the atmosphere and the top of the atmosphere (TOA). The aerosols can scatter the solar radiation reaching the ground, thus causing a cooling effect at surface, while it can also absorb the solar radiation within the atmosphere and thereby heating it. The sum of the above two is the net planetary ARF which maybe positive or negative corresponding to heating or cooling respectively. The planetary cooling or heating due to aerosol effects is a function of several parameters such as aerosol loading, optical properties, absorbing capability, relative height of aerosols and clouds, solar zenith angle, surface albedo and geographical location (e.g. Kinne and Pueschel, 2001; Hatzianastassiou et al., 2005). At any level

(surface, atmosphere, TOA) the ARF is defined by the difference of the solar fluxes with and without aerosols.

The estimation of ARF can be simplified by introducing a parameter called aerosol radiative forcing efficiency which defined as the ARF per unit change in AOD at a standard wavelength. This term is specifically important for the discrimination between absorbing and scattering aerosols. The governing equations for the calculation of ARF and ARF efficiency using SBDART model are given in the following.

Top of the atmosphere

The change in the amount of solar radiation going out of the Earth-atmosphere system due to with and without presence of aerosols is the ARF at top-of-atmosphere (TOA). The factors that define the sign of the TOA forcing are mainly the SSA, the surface albedo, the presence of clouds and the relative height between aerosol layer and clouds (Kim and Ramanathan, 2008). The radiative forcing efficiency at TOA is defined as:

$$\eta^{TOA}(\mu_0) = -\frac{F_{diff}^{TOA}(\mu_0,\tau_{550})_A - F_{diff}^{TOA}(\mu_0,\tau_{550})_{NA}}{(\tau_{550})_A - (\tau_{550})_{NA}} \quad (2.3.1)$$

where the subscripts *A* and *NA* stand for aerosols and no aerosols respectively and μ_0 is the solar zenith angle, τ_{550} is the AOD at 550 nm. The diurnal mean direct ARF efficiency at TOA (f_d^{TOA}) is given by:

$$f_d^{TOA} = \frac{S_0}{2\pi}\left[\frac{d_0}{d}\right]^2 \int_{-h_0}^{h_0} \mu_0 \eta^{TOA}(\mu_0)\, d\mu_0 \quad (2.3.2)$$

where S_0 (1367 Wm^{-2}) is the solar constant (mean solar flux per unit area at the mean Sun-Earth distance (d_0) for the perpendicular beam with μ_0=1), d is the Sun-Earth distance for the given day of the year and h_0 is the cosine of the hour angle at sunrise and sunset.

Surface

The change in the amount of total solar radiation (direct + diffuse) reaching the Earth's surface with and without the presence of aerosols is called aerosol radiative forcing (ARF) at surface. The surface ARF efficiency is defined as:

$$\eta^{SURF}(\mu_0) = \frac{F_{tot}^{SURF}(\mu_0,\tau_{550})_A - F_{tot}^{SURF}(\mu_0,\tau_{550})_{NA}}{(\tau_{550})_A - (\tau_{550})_{NA}} \quad (2.3.3)$$

The diurnal mean ARF efficiency at surface (f_d^{SURF}) is calculated by integrating the radiative forcing efficiencies $\eta^{SURF}(\mu_0)$ after weighting them with μ_0 and is given by:

$$f_d^{SURF} = \frac{S_0}{2\pi}\left[\frac{d_0}{d}\right]^2 \int_{-h0}^{h0} \mu_0 \eta^{SURF}(\mu_0) d\mu_0 \quad (2.3.4)$$

At any case the ARF at the surface is negative, since the aerosols attenuate the solar radiation when passing through the atmosphere thus causing a cooling effect at the surface. The surface ARF values depend on the amount of aerosols and their scattering and absorbing capability.

Atmosphere

The difference in radiative forcing between top of the atmosphere and surface is the net amount of radiation trapped into the atmosphere due to aerosols which defines the ARF in the atmosphere. In contrast the ARF in the atmosphere is always positive leading to atmospheric heating due to absorption of solar light by aerosols. The atmospheric ARF increases with decrease in the value of SSA.

2.3.3. Global Ozone Chemistry Aerosol Radiation and Transport

The Goddard Global Ozone Chemistry Aerosol Radiation and Transport (GOCART) model is a chemical transport model giving valuable information about the spatial distribution of aerosol types, loading and optical properties over the globe based on aerosol emissions, sources and sinks and the prevailing meteorology (Chin et al., 2002, 2009; Yu et al., 2003). The model has a horizontal resolution of 2^0 latitude by 2.5^0 longitude, 30 vertical layers and uses the assimilated meteorological fields namely wind field, temperature, pressure, specific humidity, convective cloud mass flux, cloud fraction, precipitation, boundary layer thickness, surface winds and surface wetness from the Goddard Earth Observing System Data Assimilation System (GEOS-DAS). The major aerosol types simulated in this model are: sulfate (precursors released from anthropogenic activities, biomass burning, volcanoes and oceans), dust (emitted from topographically depression regions with bare soil), organic carbon (emitted from anthropogenic, biogenic and biomass burning), black carbon (from anthropogenic and biomass burning sources) and sea-salt (emitted from the oceans). These aerosols undergo various dynamical processes in the atmosphere and therefore, the model includes the advection, convection, dry deposition, settling, wet deposition and hygroscopic growth of the aerosols (Chin et al., 2001). In this study, the GOCART simulations (total AOD, dust AOD) are used over South Asia (*described in section 5.7.5*) in order to investigate the trends of aerosols over the last decade and to compare the model simulations with the MODIS observations.

2.3.4. Hybrid Single-Particle Lagrangian Integrated Trajectory

The Air Resources Laboratory's HYbrid Single-Particle Lagrangian Integrated Trajectory (HYSPLIT) model is a complete system for computing both simple air parcel trajectories, complex dispersion and deposition simulations. The model calculation method is a hybrid between the Lagrangian approach which uses a moving frame of reference as the air parcels move from their initial location and the Eulerian approach which uses a fixed three-dimensional grid as a frame of reference. In the model advection and diffusion calculations are made in a Lagrangian framework following the transport of the air parcel, while pollutant concentrations are calculated on a fixed grid. The model uses advection algorithms updated stability and dispersion equations, a graphical user interface and the option to include modules for chemical transformations Draxler and Rolph (2003). The backward air-mass trajectories are of major interest in order to study the aerosol origin and transport pathways. In the present study, the HYSPLIT model is used for the computation of backward air-mass trajectories over Hyderabad and BoB. Since the trajectory model is subjected to uncertainty arising from interpolation on sparse meteorological data assumptions regarding the vertical transport, observational errors. The uncertainty involved in their calculation needs to be considered when interpreting the individual trajectories; therefore this study adopted the clustering of air trajectories to identify the possible advection pathways of atmospheric aerosols. HYSPLIT provides valuable information about the pathways and altitude variation of the air masses arriving over a specific location.

2.4 Trace Gases Analyzers

2.4.1 Ozone Analyzer

Ozone analyzer (*Thermo Scientific*; *Model 49i*) was used for surface Ozone analysis. It is based on UV-photometric technique and the degree to which the UV light is absorbed is directly related to the Ozone (O_3) concentration as described by the Beer-Lambert law which defines how the light of a specific wavelength is absorbed by a particular gas molecule over a certain distance at a given temperature and pressure

$$I = I_0 \exp[-\sigma(\lambda)lc] \qquad \text{at STP} \qquad (2.4.1)$$

Since the concentration of the sample ozone gas is strongly dependent on both temperature and pressure at the sampling site, correction needs to be applied. After applying the correction factor, the equation is modified as:

$$C = \ln(\frac{I}{I_0})(\frac{10^{-9}}{\alpha l})(\frac{T}{273^0 K})(\frac{29.92 inHg}{P}) \quad (2.4.2)$$

Where I and I_0 are the UV light intensity with and without ozone respectively, β is the molecular absorption coefficient ($308cm^{-1}$ at 0 ^{0}C and 1 atmosphere), l length of measuring cell, c is the ozone concentration in ppb.

2.4.2 NOx Analyzer

NOx Analyzer (*Thermo Scientific*; *Model 42i*) is designed to measure the concentration of nitrogen oxide (NO), total oxides of nitrogen (NOx) by calculation of nitrogen dioxide [NO_2] based on the principle that the reaction of NO with O_3 results in electronically excited NO_2 molecules and which releases their excess energy by emitting a photon and dropping to a lower energy level. The characteristics luminescence that produced is linearly proportional to the NO concentration.

$$NO + O3 \rightarrow NO_2^* + O_2 \quad (2.4.3)$$
$$NO_2^* \rightarrow NO_2 + hv \quad (2.4.4)$$

Nitrogen dioxide (NO_2) must be transferred into NO before it can be measured using the chemiluminescent reaction.NO_2 is converted to NO by a molybdenum converter (NO_2 –to-NO) heated to about 325^0C.

$$3NOx + Mo \rightarrow 3NO + MoO_3 \quad (2.4.5)$$

2.4.3 CO Analyzer

CO Analyzer (*Thermo Scientific*; *Model 48i*) measures the carbon monoxide by comparing infrared energy absorbed by a sample to that absorbed by a reference gas as per the Beer-Lambert law by virtue that the carbon monoxide (CO) absorbs infrared radiation (IR) at 4.6µm. Since the IR measurement is non- linear measurement technique and therefore, it is necessary to transform the basic analyzer signal into a linear output. However, an internal stored calibration curve is used to accurately linearize the instrument output over range up to a concentration of 10, 000ppm.

2.4.4 SO_2 Analyzer

SO_2 Analyzer (*Thermo Scientific*; *Model 43i*) operates on the principle that SO_2 molecules absorb ultraviolet (UV) light and become excited at one wavelength then decay to a lower energy state emitting UV light at a different wavelength that is proportional to the SO_2 concentration.

$$SO_2 + hv_1 \rightarrow SO_2^* + hv_2 \quad (2.4.6)$$